Time-resolved study of phonon polaritons in $LiTaO_3$

H. J. Bakker, S. Hunsche, and H. Kurz
Institute for Semiconductor Electronics II, Rheinisch-Westfälische Technische Hochschule Aachen, D-52056 Aachen, Germany
(Received 29 April 1993; revised manuscript received 8 July 1993)

We study the temperature dependence of the low-frequency dielectric properties of the ferroelectric $LiTaO_3$ by generating phonon polaritons with frequencies in the terahertz regime. The phonon polaritons are impulsively excited and phase-sensitively detected with 60-fs laser pulses. The propagation and damping of the polaritons are investigated as a function of frequency and temperature. The experimental results are compared with a quantum-mechanical model for the low-frequency dielectric response of $LiTaO_3$. In this model the lowest-energy A_1 mode is described with a one-dimensional anharmonic potential in a single unit cell. We find that at 300 K the polariton dispersion and damping are determined by a strong resonance at 6 THz and a weak resonance at 1 THz. The latter resonance is due to a tunneling transition and leads to the observation of phonon-polariton beats. The model predicts that with increasing temperature the strength of the resonance at 6 THz decreases and that a new broad resonance at 3 THz and a central mode arise. The measured polariton dispersion and damping are in quantitative agreement with these theoretical predictions. Thereby we obtain evidence that the ferroelectric phase transition in $LiTaO_3$ takes place without mode softening.

I. INTRODUCTION

When light propagates through a medium with resonances, the coupling between light and polarization leads to the formation of new mixed light-polarization states. These new states are called polaritons. Clearly, polaritons form a very general type of excitation. The study of polaritons gives information on the nature of the light-matter interaction and on the properties of the material resonances to which the light is coupled. The effects of the coupling between light and material resonances is most clearly observed in the dispersion. When the light frequency approaches the frequency of a resonance, the coupling leads to an avoided crossing in the dispersion of the polaritons. As a result, a lower and an upper polariton-dispersion branch appear.[1] Far away from the avoided crossing, one of the two polaritons at a given wave vector will be strongly lightlike and propagates with the velocity of light while the other will be strongly polarizationlike and hardly propagates. Near the avoided crossing, the polaritons are strongly dispersive, leading to strong spreading and damping of polariton wave packets upon propagation.

Low-frequency phonon polaritons can be excited with visible light by cw Raman scattering[2–4] or nonlinear optical techniques such as impulsive stimulated Raman scattering (ISRS),[5–8] difference-frequency mixing,[9,10] coherent anti-Stokes Raman scattering (CARS),[11,12] and the optical Čerenkov effect.[13] Visible light can only be used for the excitation of phonon polaritons in noncentrosymmetric materials. Only in these materials can the phonons be simultaneously Raman and infrared active. The Raman activity is required to excite the phonon polariton via the Raman effect. The infrared activity is required to get a strong electric-dipole coupling of the phonon to light. This coupling is a prerequisite for the formation of polaritons. If the phonon polaritons are excited by difference-frequency mixing or the optical Čerenkov effect, the material also has to be noncentrosymmetric because these second-order nonlinear optical processes can only take place in materials that have no center of inversion.

The availability of ultrashort laser pulses allows the time-resolved study of the dynamics of polaritons. In addition, due to their large bandwidth, short pulses allow the simultaneous excitation of polaritons of the lower and upper branches of the dispersion so that polariton beats can be observed.[9,14] Previous time-resolved studies on $KNbO_3$, $BaTiO_3$, and $LiNbO_3$[6,7,15] showed that valuable information on the nature of the ferroelectric phase transition can be obtained from the measurement of the polariton dispersion at different temperatures.

A previous cw Raman study on phonon polaritons in ferroelectric $LiTaO_3$ showed that the polariton dispersion is strongly influenced by the lowest-energy TO phonon of A_1 symmetry with a resonance frequency of 6 THz at 300 K. This study also revealed an anomaly in the dispersion at low frequencies.[2] It was observed that the dispersion flattens out for small wave vectors so that the polariton frequency seems to saturate. It was suggested that bulk polaritons with frequencies below 1.4 THz cannot exist due to crystal-domain variations. However, in a recent time-resolved study it was found that this anomaly was due to the presence of a weak resonance at 1 THz and bulk polaritons with frequencies down to 0.5 THz were observed in $LiTaO_3$.[9]

The phonon with a frequency of 6 THz at 300 K is the so-called ferroelectric mode, because it plays an important role in the ferroelectric phase transition. This mode is mainly formed by the oscillation of the Li^+ ion along the optical axis. The frequency and strength of this mode

are found to be strongly temperature dependent.[16,17] $LiTaO_3$ undergoes a phase transition from the ferroelectric to the paraelectric phase at $T_c = 890$ K (Curie temperature). For temperatures close to T_c a strong resonance near frequency zero is observed (central mode).[3] The presence of this central mode complicates the experimental determination whether the frequency of the TO phonon shifts to zero (mode softening) on approaching the Curie temperature or not. In some experimental studies on $LiTaO_3$ the phonon was found to be soft,[16,17] whereas in other studies no mode softening was observed.[3,18]

In this paper we investigate the temperature dependence of the dispersion and damping of phonon polaritons in $LiTaO_3$. The experimental results will be interpreted with a quantum-mechanical model for the low-frequency dielectric response in $LiTaO_3$. This model also provides an accurate description of the ferroelectric phase transition.[19]

This paper is organized as follows. In Sec. II we describe the experimental setup and we give a theoretical description for the impulsive excitation and phase-sensitive detection of phonon polaritons. In Sec. III we describe the quantum-mechanical model for the low-frequency dielectric response of $LiTaO_3$ and we show how this model can be used to calculate the polariton response. The experimental and calculated results are presented and discussed in Sec. IV. Finally, Sec. V presents the conclusions.

II. EXPERIMENT

A. Experimental setup

The experimental setup used for the generation and detection of phonon polaritons is presented in Fig. 1. The experiments are performed using the pulses from a colliding pulse mode-locked (CPM) laser that are amplified in a six-pass dye amplifier pumped by the 510.5 nm line of a Cu-vapor laser.[20] The generated pulses have an energy of 5 μJ, a pulse duration of 60 fs, a central wavelength of 625 nm, and a repetition rate of 6.8 kHz. The amplified pulses are split into two strong pump pulses

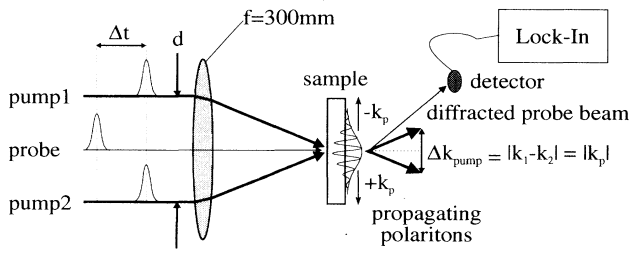

FIG. 1. Experimental setup for the generation and detection of phonon polaritons. The polaritons are generated via difference-frequency mixing of two intense pulses with a pulse duration of 60 fs, an energy of 2 μJ, and a central wavelength of 625 nm. The polaritons are probed via diffraction of a third delayed probe pulse.

of approximately equal power and a weak probe pulse. All three pulses are focused by the same lens (f=30 cm) to a focus of about 200 μm into a 2 mm thick $LiTaO_3$ crystal. The spatial intensity distribution of the beams is near-Gaussian and the focus diameter of each beam is determined from the fraction of light that is transmitted through a calibrated pinhole centered at the focus. The pump pulses have a common focus and enter the crystal simultaneously. Temporal and spatial overlap of these pulses is easily determined from the self-diffraction of these pulses that is visible to the naked eye. The pump pulses generate low-frequency polaritons via a nonlinear interaction that generates a polarization at the difference frequency of the two pump pulses. This nonlinear interaction can be difference-frequency mixing which is a second-order nonlinear optical process or stimulated Raman scattering which is a third-order nonlinear optical process. The nonlinear polarization that results from difference-frequency mixing leads to the excitation of phonon polaritons over their light character. Hence this excitation will be most efficient for polaritons that have strong light character. If the polaritons are excited by stimulated Raman scattering, the generated nonlinear polarization is formed by the excitation of the phonon part of the polariton so that this excitation process will be most efficient when the polaritons have strong phonon character. In the case of $LiTaO_3$ the second-order susceptibility is very large so that at almost all frequencies the phonon polaritons are predominantly excited by difference-frequency mixing. The nonlinear interaction leads to the generation of a nonlinear polarization with a wave vector that is given by the difference of the wave vectors of the two pump beams. Hence, the angle between the two pump beams determines the wave vector for which the nonlinear optical process is phase matched. The polariton frequencies that correspond with this wave vector are generated with the highest efficiency out of the broad bandwidth (10 THz) of the pump pulses. The wave vector can be varied by adjusting the distance between the two pump beams at the lens.

The optical axis of the $LiTaO_3$ crystal is oriented perpendicular to the plane of incidence. The pump pulses are polarized along the optical axis in order to obtain the highest effective second-order susceptibility. This generation can be characterized as impulsive because the pump-pulse duration is much shorter than the polariton oscillation period. This excitation produces counterpropagating phonon polaritons with well-defined wave vector and phase. The wave vector and the direction of propagation of the polaritons are practically perpendicular to the wave vectors of the two pump beams, because the two pump pulses have equal central wavelengths.

The polaritons are probed with the third pulse using the linear electro-optic effect. Time-delay zero between probe and the two pumps can be recognized from the strong four-wave mixing signal of electronic origin that arises when the probe and the two pumps have temporal and spatial overlap. The electric field associated with the polaritons strongly modulates the refractive index. The resulting index grating diffracts the probe that is polarized along the optical axis. We measure the first-

order diffracted light intensity as a function of the delay between the probe and the two pump pulses. This measurement provides information on the frequency, propagation, and damping of the generated polaritons. The diffracted signal is detected using a lock-in technique in which the diffracted signal is modulated with 3.4 kHz by chopping either the probe or the pump beams with a chopper that is synchronized to the copper-vapor laser.

B. Generation of phonon polaritons via difference-frequency mixing

Polaritons are mixed light-polarization states that arise as a result of the coupling of light with material resonances. The dynamics of the polaritons can be described with the coupled Maxwell-Bloch equations. The light is described with the wave equation derived from Maxwell's equations, the material resonances with the optical Bloch equations for the polarization, and the population of a multilevel system. The coupling arises due to the fact that a polarization generates an electromagnetic field and an electromagnetic field can generate a polarization if the transition-dipole moments are nonzero.

In our experiment the polaritons are excited via a nonlinear interaction of two ultrashort laser pulses with the same central frequency. In the case of $LiTaO_3$ this nonlinear interaction is mainly formed by a difference-frequency mixing process. The resulting nonlinear polarization acts as a source of electromagnetic radiation in the wave equation. The nonlinear polarization at the difference frequency is given by

$$\mathcal{P}_{\mathrm{NL}} = \chi^{(2)}\mathcal{E}_1\mathcal{E}_2^*. \tag{2.1}$$

The electric field $\mathcal{E}_j$ of laser pulse j can be written as $E_j\cos(k_jz-\omega_jt)$ with the amplitude function E_j given by the square root of the pulse envelope function.

When this nonlinear source term is introduced in the wave equation and the slowly-varying-amplitude and the rotating-wave approximations are used, the wave equation takes the following form:

$$\left(\frac{\partial}{\partial z}+\frac{1}{v_g}\frac{\partial}{\partial t}\right)E_p = \frac{-i}{2\epsilon_0 c n_\infty \omega}\left\{\frac{\partial^2 P_p}{\partial t^2} - 2i\omega\frac{\partial P_p}{\partial t} - \omega^2 P_p + e^{i\omega t}\chi^{(2)}\frac{\partial^2 E_1E_2^*}{\partial t^2}\right\}, \tag{2.2}$$

with the electric field of the polariton $\mathcal{E}_p(z,t)$ defined by $E_p(z,t)\cos(k_pz-\omega t)$, the polarization of the polariton $\mathcal{P}_p(z,t)$ defined by $P_p(z,t)\cos(k_pz-\omega t)$, k_p $(=k_1-k_2)$ the wave vector of the polariton, ω the light frequency $(\omega = ck_p/n_\infty)$, n_∞ the refractive index, v_g the group velocity, c the velocity of light in vacuum, and $\chi^{(2)}$ the second-order susceptibility. The polarization P_p entering these equations is the polarization that is associated with the resonances with frequencies near the light frequency. The parameters n_∞, v_g, and ω represent the refractive index, the group velocity, and the angular frequency *without* taking into account the interaction with the resonances leading to polarization P_p. The actual refractive index, group velocity, and frequency of the polaritons are strongly affected by this polarization. In principle polaritons at all frequencies within the bandwidth of the ultrashort laser pulses can be generated. However, the polariton frequencies that correspond to the wave vector k_p according to the polariton dispersion will be generated with the highest efficiency. Hence by varying ω $(=ck_p/n_\infty)$ in Eq. (2.2), the polariton frequencies that result from the coupling of Eq. (2.2) to the Bloch equations are changed.

Equation (2.2) describes the generation of polaritons with wave vector k_p. In our experiment also an equally intense counterpropagating polariton is generated with wave vector $-k_p(=k_2-k_1)$, due to the fact that the central wavelengths of the two laser pulses are equal. The electric field of this second polariton is given by $E_p\cos(-k_pz-\omega t)$ and the polarization by $P_p\cos(-k_pz-\omega t)$. The wave equation for this polariton is similar to Eq. (2.2), but with $-\partial/\partial z$ instead of $\partial/\partial z$ and $E_1^*E_2$ instead of $E_1E_2^*$.

C. Probing of polaritons via the linear electro-optic effect

In our experiment the generated counterpropagating polariton wave packets are probed via diffraction of a probe beam from the index grating formed by the polaritons as a result of the linear electro-optic effect. The periodicity of this index grating is given by the wave vector of the polariton. The linear electro-optic effect induces a change of the refractive index that is linearly proportional to the electric fields of the polaritons. Hence, the resulting index grating has the same dependence on z and t as the polaritons. The spatial profile of the polaritons is given by the product of the (Gaussian) profiles of the two pump beams. The two counterpropagating polaritons can be described as follows:

$$\mathcal{E}_p(z,t)(\pm) = E_{p0}e^{-\frac{(z\mp v_{gp}t)^2}{\Delta z_{pu}^2}}\cos(k_pz\mp\omega_pt)e^{-\frac{t}{T_{2p}}}, \tag{2.3}$$

with $(\pm)$ denoting the two counterpropagating polaritons, E_{p0} the electric-field amplitude, v_{gp} the group velocity, ω_p the angular frequency, and T_{2p} the exponential damping-time constant of the polaritons. The spatial intensity distribution of the pump pulses is given by $e^{-\frac{z^2}{\Delta z_{pu}^2}}$. The angular distribution of the diffracted probe field is given by the Fourier transform of the grating formed by the polaritons multiplied with the spatial intensity distribution of the probe. Hence, the diffracted electric field of the probe in the direction k can be described by the following Fourier integral:

$$\mathcal{E}_p(k,t)(\pm) = E_{p0} e^{-\frac{t}{T_{2p}}} \int e^{-\frac{(z-z_{pr})^2}{2\Delta z_{pr}^2}} e^{-\frac{(z\mp v_{gp}t)^2}{\Delta z_{pu}^2}} \frac{1}{2}\left(e^{i(k_p z \mp \omega_p t)} + \text{c.c.}\right) e^{-ikz} dz, \tag{2.4}$$

with $e^{\frac{-(z-z_{pr})^2}{\Delta z_{pr}^2}}$ the spatial intensity distribution of the probe. The probe is shifted z_{pr} with respect to the excitation spot. In this equation it is assumed that the probe pulse propagates parallel to the two pump beams so that its position with respect to the excited spot is time independent. If we only consider diffracted electric fields with k vectors near k_p, the complex conjugate in Eq. (2.4) can be omitted. Evaluation of the integral in Eq. (2.4) gives

$$\mathcal{E}_p(k,t)(\pm) \propto e^{\mp i\omega_p t - \frac{v_{gp}^2 t^2}{\Delta z_{pu}^2} - \frac{z_{pr}^2}{2\Delta z_{pr}^2} - \frac{t}{T_{2p}}} e^{\left\{\frac{v_{gp}^2 t^2}{\Delta z_{pu}^4} + \frac{z_{pr}^2}{4\Delta z_{pr}^4} - \frac{(k-k_p)^2}{4}\right\}\left\{\frac{2\Delta z_{pr}^2 \Delta z_{pu}^2}{2\Delta z_{pr}^2 + \Delta z_{pu}^2}\right\}}$$
$$\times e^{\left\{\mp\frac{iv_{gp}(k-k_p)t}{\Delta z_{pu}^2} - \frac{iz_{pr}(k-k_p)}{2\Delta z_{pr}^2} \pm \frac{z_{pr} v_{gp} t}{\Delta z_{pu}^2 \Delta z_{pr}^2}\right\}\left\{\frac{2\Delta z_{pr}^2 \Delta z_{pu}^2}{2\Delta z_{pr}^2 + \Delta z_{pu}^2}\right\}}. \tag{2.5}$$

When $\Delta z_{pr} = \frac{1}{2}\sqrt{2}\Delta z_{pu}$, Eq. (2.5) simplifies to

$$\mathcal{E}_p(k,t)(\pm) \propto e^{\mp i\left(\omega_p + \frac{1}{2}v_{gp}(k-k_p)\right)t - \frac{(v_{gp}t \mp z_{pr})^2}{2\Delta z_{pu}^2} - \frac{(k-k_p)^2 \Delta z_{pu}^2}{8} - \frac{t}{T_{2p}} - \frac{1}{2}iz_{pr}(k-k_p)} \tag{2.6}$$

This expression shows that the intensity of the diffracted signal has a Gaussian time dependence. This time dependence follows from the propagation of the polaritons through the spatial region of the probe. The maximum of the signal is attained at $t = z_{pr}/v_{gp}$ for the + polariton and at $t = -z_{pr}/v_{gp}$ for the − polariton. In addition, this expression shows that the phase evolution of $\mathcal{E}_p(k,t)$ depends on k via $\omega(k) = \omega_p + \frac{1}{2}v_{gp}(k-k_p)$. This implies that care should be taken that the polariton frequency is always determined at $k = k_p$, which corresponds with the maximum of the diffraction. This expression also shows that the diffracted intensity depends on k via $e^{-\frac{(k-k_p)^2\Delta z_{pu}^2}{8}}$. It follows that the width of the diffraction angle is inversely proportional to the spatial width of the polariton.

Equations (2.5) and (2.6) show that for each separate polariton wave packet only the phase of $\mathcal{E}_p(k,t)$ evolves with the polariton frequency and that the intensity of the diffracted field, given by $|\mathcal{E}_p(k,t)|^2$, does not depend on frequency. As a consequence, the polariton frequency cannot be observed in our time-resolved pump-probe experiments, unless there are certain interference effects. One of these effects is the interference of the diffracted electric field with background scattered probe light that has a delay-independent phase. There will always be some background scattered probe light as a result of inhomogeneities. In the presence of background scattered light the total intensity $I_t(k,t)$ in the direction of diffraction is given by

$$I_t(k,t) = |\mathcal{E}_p(k,t)|^2 + |\mathcal{E}_b(k)|^2 + \mathcal{E}_p(k,t)^*\mathcal{E}_b(k) + \mathcal{E}_p(k,t)\mathcal{E}_b(k)^*, \tag{2.7}$$

with $\mathcal{E}_b$ the electric field of the background scattered light. Only the last two terms in Eq. (2.7) will oscillate with the polariton frequency. Equation (2.7) shows that when $\mathcal{E}_b(k) \gg \mathcal{E}_p(k,t)$, the time-dependent part of the total intensity in the diffracted direction will be linearly proportional to $\mathcal{E}_p(k,t)$ and that this intensity will be modulated with the single-polariton frequency. As a result, the polariton frequency can be obtained from the Fourier transform of the time-resolved measurements. The interference with a strong background scattered electric field also makes that the time-dependent part of the intensity in the diffracted direction decays with a time constant T_{2p} instead of $T_{2p}/2$.

Another interference effect is the interference of the two counterpropagating polaritons with each other. For $z_{pr} = 0$, meaning that the probe is focused at the same spot as the two pump beams, the diffracted signals of the polaritons have equal intensity and the observed signal is strongly influenced by their interference. The total diffracted electric field that follows from the sum of the diffraction of the two counterpropagating polaritons is given by

$$\mathcal{E}_p(k,t) \propto e^{-\frac{v_{gp}^2 t^2}{2\Delta z_{pu}^2} - \frac{(k-k_p)^2\Delta z_{pu}^2}{8} - \frac{t}{T_{2p}}} \times \cos\left\{\left(\omega_p + \frac{1}{2}v_{gp}(k-k_p)\right)t\right\}. \tag{2.8}$$

The diffracted intensity is equal to

$$I_p(k,t) \propto e^{-\frac{v_{gp}^2 t^2}{\Delta z_{pu}^2} - \frac{(k-k_p)^2\Delta z_{pu}^2}{4} - \frac{2t}{T_{2p}}} \times \left(\frac{1}{2} + \frac{1}{2}\cos\left\{2\left(\omega_p + \frac{1}{2}v_{gp}(k-k_p)\right)t\right\}\right). \tag{2.9}$$

It follows from this equation that the diffracted intensity of two counterpropagating polaritons is modulated with twice the polariton frequency.

Equation (2.9) is valid when the polaritons are well described by Eq. (2.3), which means that the polariton frequency should be well defined. However, the impulsive generation with large bandwidth and fixed wave vector can lead to the excitation of phonon polaritons

of two or more polariton-dispersion branches. Far away from the avoided crossing in the dispersion, the two excited polariton-dispersion branches have strongly different electric-field amplitudes and group velocities so that their interference will only lead to a small additional modulation of the total diffracted signal. In this limit the lightlike polariton-dispersion branch will be predominantly observed. However, for wave vectors near the avoided crossing, the electric fields and the group velocities of the polariton-dispersion branches become similar so that their interference will lead to a strong modulation of the diffracted signal.

In the following we will denote the excited polariton frequencies as the polariton response. If the polariton response contains many frequency components, the sum of the diffracted electric fields of two counterpropagating polaritons can be written as a sum of many cosines:

$$\mathcal{E}_p(k,t) \propto e^{-\frac{v_{gp}^2 t^2}{2\Delta z_{pu}^2} - \frac{(k-k_p)^2 \Delta z_{pu}^2}{8} - \frac{t}{T_{2p}}} \times \sum_m C_m \cos\left\{\left(\omega_{mp} + \frac{1}{2} v_{gp}(k-k_p)\right)t\right\}, \tag{2.10}$$

with C_m a coefficient indicating the contribution of frequency component ω_{mp}. In this equation it is assumed that the group velocity is the same at all frequencies. If the polariton response contains frequencies belonging to two different dispersion branches, this will in general not be a good assumption. On the other hand, the two dispersion branches will only both be important if they are excited with approximately the same amplitude and are about equally lightlike. In that case the group velocities will also be rather similar. The diffracted intensity is given by

$$I(k,t) \propto e^{-\frac{v_{gp}^2 t^2}{\Delta z_{pu}^2} - \frac{(k-k_p)^2 \Delta z_{pu}^2}{4} - \frac{2t}{T_{2p}}} \sum_{m,n} C_m^* C_n \frac{1}{2}\left\{\cos\left(\omega_{mp} - \omega_{np}\right)t + \cos\left[\omega_{mp} + \omega_{np} + v_{gp}(k-k_p)\right]t\right\}. \tag{2.11}$$

This expression shows that the diffracted intensity contains the sum and difference frequencies of all excited polariton frequencies, weighted with the product of the corresponding coefficients. The maximum frequency of the diffracted intensity can differ from twice the maximum frequency of the polariton response. When the polariton response has two narrow maxima at ω_1 and ω_2, the Fourier transform of the signal as given by Eq. (2.11) will peak at frequencies 0, $\omega_2-\omega_1$, $2\omega_1$, $\omega_1+\omega_2$, and $2\omega_2$. In that case ω_1 and ω_2 can be derived from the Fourier transform of the time-resolved measurement. However, when the peaks in the polariton response at ω_1 and ω_2 are very broad and overlap, the peaks in the Fourier transform of the signal as given by Eq. (2.11) can no longer be resolved. In the low-frequency regime, the Fourier transform of the signal will have a maximum at frequency zero and will slowly decrease with increasing frequency. This implies that when the polariton response contains several broad and overlapping peaks, it is not possible to determine the frequencies of these maxima in an experiment in which the probe is diffracted from two counterpropagating polaritons. In the high-frequency regime, the Fourier transform of the signal still peaks at about $\omega_1+\omega_2$. This maximum will shift to somewhat higher frequencies when the polariton response is stronger at ω_2 than at ω_1 and to lower frequencies when the polariton response is stronger at ω_1 than at ω_2. Therefore this peak corresponds rather well to twice the average polariton frequency.

D. Simulation of experiment

The time-resolved measurements at different wave vectors give information on the frequency and the damping of the phonon polaritons. The polariton frequency can be obtained from a Fourier transform of the time-resolved measurements. In most experiments both the polariton frequency is observed as a result of the interference with background scattered probe light and the double polariton frequency as a result of the interference of the counterpropagating polaritons. The derivation of the damping from the time-resolved measurements is more complicated because the measured decay of the signal is caused both by propagation and damping of the polaritons. To derive a time constant for the damping, we perform a simulation of the time-resolved measurements. In this simulation both the effects of propagation and damping are accounted for. The two counterpropagating polaritons are described with Eq. (2.3). The group velocity v_{gp} that enters this equation is obtained from the measured polariton dispersion using $v_{gp} = \frac{\partial \omega_p}{\partial k_p}$. We calculate the Fourier transform of the index grating that is induced by the polaritons [Eq. (2.5)] as a function of the delay between pump and probe. In the simulation also the interference with background scattered probe light is taken into account.

III. QUANTUM-MECHANICAL CALCULATION OF THE LOW-FREQUENCY DIELECTRIC RESPONSE OF $LiTaO_3$

A. Quantum-mechanical model for $LiTaO_3$

In this subsection we describe a quantum-mechanical model for the ferroelectric mode of $LiTaO_3$. This model can be used to describe the ferroelectric phase transition in $LiTaO_3$.[19] In this paper we will use this model to describe the temperature dependence of the dielectric function and the polariton response. In this model the vibrational states of the lowest-energy TO phonon of A_1 symmetry (ferroelectric mode) are calculated using a one-dimensional potential that describes the energy in a single unit cell.[21] We assume that the frequencies of the transitions between the vibrational levels are not influenced by the wave vector. This means that the effects of

dispersion of the phonon are neglected. This should be a good assumption in the wave vector regime in which we investigate the polaritons. The polaritons that arise from the coupling of the phonon with the electromagnetic field are still strongly dispersive.[1]

The one-dimensional potential that we use for the description of the vibrational states is a function of the vibrational normal coordinate r along the optical axis. The expectation value $\langle r \rangle$ of this coordinate is proportional to the displacement of the ions from their centrosymmetric positions and defines the mean polarization of the unit cell. The normal vibration is mainly formed by the oscillation of the Li^+ ion along the optical axis. We use a mean-field approach and take the spontaneous polarization of the whole crystal equal to the polarization of this single unit cell. This spontaneous polarization forms the local electric field and leads to a contribution to the potential that is proportional to $\langle r \rangle r$.

We will describe the lowest-energy A_1 phonon in $LiTaO_3$ with a potential that contains three minima.[19] This agrees with the experimental observation that above T_c the Li^+ ion is not only found at the centrosymmetric position but also at positions ± 0.037 nm displaced along the optical axis.[22] It also agrees with a previous classical calculation in which the dielectric parameters of $LiTaO_3$ are described with an extremely anharmonic potential that contains three minima.[23] The used potential is adjusted to a few experimental data. The positions of the three minima of the potential are adjusted to the positions of the Li^+ ion in the unit cell above T_c. The curvature of the potential is chosen such that it reproduces the measured absorption spectrum at 300 K, containing a strong resonance at 6 THz. The two outer wells of the potential are described with a Morse potential and the central well with a harmonic potential. The potential energy is given in atomic units (1 a.u. = 219483.9 cm^{-1}) as a function of the normal mode coordinate r in atomic units. The dimension of r is length times square root of mass. The potential including the local electric field has the following form:

$$V(r) = \begin{cases} 4.75 \times 10^{-2} \times (e^{-3.39 \times 10^{-3}(r-169.4)} - 1)^2 + 3.395 \times 10^{-2} \langle r \rangle r & \text{if } |r| > 101 \text{ a.u.}, \\ 4.15 \times 10^{-7} \times r^2 + 3.395 \times 10^{-2} \langle r \rangle r & \text{if } |r| < 56 \text{ a.u.} \end{cases} \tag{3.1}$$

The three different parts of this potential are interconnected by a cubic spline. For $\langle r \rangle = 0$, the frequencies of the harmonic parts are 200 cm^{-1} for the middle well and 229 cm^{-1} for the two outer wells. This potential does not depend explicitly on temperature. However, it depends indirectly on temperature through the value of $\langle r \rangle$.

The value for $\langle r \rangle$ at a particular temperature is calculated in a self-consistent way. Assuming a certain value for $\langle r \rangle$, the potential (3.1) is used in the one-dimensional vibrational Schrödinger equation

$$\left(-\frac{\hbar^2}{2} \frac{\partial^2}{\partial r^2} + V(r) \right) \phi_{\text{vib}}(r) = E_{\text{vib}} \phi_{\text{vib}}(r), \tag{3.2}$$

with E_{vib} the vibrational energy and $\phi_{\text{vib}}(r)$ the vibrational wave function. This equation is solved numerically with the Numerov method.[24] At each temperature we calculate the lowest 50 vibrational levels. For each of these levels the expectation value of r is given by $\langle \phi_{\text{vib}} | r | \phi_{\text{vib}} \rangle$. Using a normalized Boltzman distribution for the occupation of the levels, a new value for $\langle r \rangle$ is calculated taking all levels into account. With this new $\langle r \rangle$ the calculation of the potential and the levels is repeated until convergence is reached. With increasing temperature the value of $\langle r \rangle$ decreases until at the Curie temperature this value becomes equal to zero. The calculation of $\langle r \rangle$ at different temperatures gives the temperature dependence of the spontaneous polarization.

The static dielectric response is also calculated in a self-consistent way by calculating the change of the value of $\langle r \rangle$ upon adding a small term Er to the potential where E represents a small static electric field.

In Fig. 2 the potential energy curves at 300 K and 733 K and the 19 lowest-energy vibrational wave functions in these potentials are presented as a function of the displacement of the Li^+ ion. The displacement of the Li^+ ion is linearly proportional to the coordinate r of the normal vibration. Due to the nonzero value of the mean displacement, the potential is tilted so that the minima of the three wells have different energies. The potential is much less tilted at 733 K than at 300 K because $\langle r \rangle$ decreases with increasing temperature. This decrease is due to the increasing occupation of higher-energy delo-

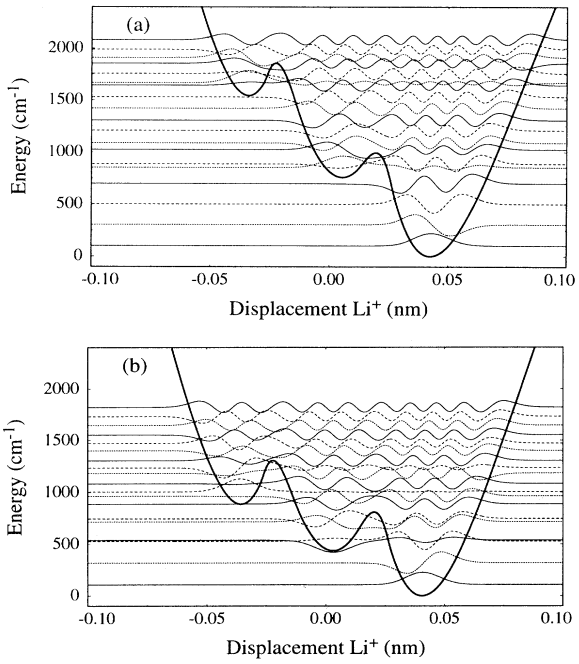

FIG. 2. Potential-energy curves and the 19 lowest-energy vibrational wave functions for the lowest-energy A_1 mode in one unit cell of $LiTaO_3$ as a function of the displacement of the Li^+ ion along the optical axis. (a) 300 K ($\langle r \rangle = 0.043$ nm); (b) 733 K ($\langle r \rangle = 0.025$ nm).

calized vibrational levels with small values for $\langle r \rangle$ with increasing temperature. This effect is further amplified by the fact that due to the smaller tilt of the potential less vibrational energy is required to make a vibrational wave function delocalized.

B. Calculation of the dielectric function and the polariton response

In the previous subsection it was shown how the quantum-mechanical model can be used to calculate the static dielectric response. This static dielectric response of the crystal can be seen as the sum of two contributions.

The first contribution is the direct change in the polarization that follows from the change of the vibrational wave functions when the potential is tilted by adding a term Er. In this direct contribution it is assumed that the term in the potential that is proportional to $\langle r \rangle r$ does not change. It can be shown via perturbation theory that for small electric fields this direct contribution to the polarization is equal to the static dielectric response that follows from the transitions between the vibrational levels in the potential of the single unit cell. This contribution to the static dielectric constant will be referred to in the following as direct single-unit-cell response.

The change in the polarization of each single unit cell implies that the value of $\langle r \rangle$ changes which leads to a change of the term in the potential that is proportional to $\langle r \rangle$. This change in the mean field induces a further tilt of the potential and a further increase of the polarization. This latter indirect effect forms the second contribution to the static dielectric response. This effect becomes very strong near T_c and causes the observed divergence of the static dielectric constant at T_c.[19] A change in the value of $\langle r \rangle$ implies that the probability distribution in the three wells has to change. This means that the ions (mainly the Li^+ ion) have to be transported through the barriers that separate the wells of the potential. This transport through the potential will take some time so that this indirect contribution to the response will be slow compared to the direct single-unit-cell response. The indirect contribution due to the change in $\langle r \rangle$ will be referred to in the following as indirect mean-field response.

The frequency dependence of the direct single-unit-cell response is described with the dielectric-response function that follows from the optical Bloch equations for a multilevel system:

$$\epsilon_{\mathrm{SU}}(\omega) = \sum_{i,j} \frac{2(N_i - N_j)e^2|\mu_{ij}|^2\omega_{ij}/(\epsilon_0\hbar)}{\omega_{ij}^2 - \omega^2 - \frac{2i\omega}{T_{2,ij}}}, \qquad (3.3)$$

with the indices i and j indicating a vibrational level, N_i and N_j the populations of these levels, μ_{ij} the transition-dipole moment between level i and level j, $\hbar\omega_{ij}$ the energy difference between levels i and j, and $T_{2,ij}$ the damping-time constant associated with this transition. At frequency zero this response is exactly equal to the response that results from the calculation of the change in the vibrational wave functions upon adding a small term Er to the potential and taking the term proportional to $\langle r \rangle r$ constant.

The frequency dependence of the indirect mean-field response is more complicated. At frequency zero this response should exactly equal the indirect contribution to the static dielectric constant that results from the change in the mean field. It can be expected that the mean-field response can only follow the oscillations of an applied electromagnetic fields at low frequencies. At high frequencies, the transport of probability through the barriers of the potential will be too slow to follow the oscillations of the electric field, so that the full mean-field response to the electric field will not be attained. Hence, the indirect mean-field response possesses a finite linewidth meaning that at high frequencies this contribution to the dielectric response becomes negligible. As a result of the decrease in the mean-field response with increasing frequency, the static dielectric constant that is measured with capacitance measurements can be much higher than the static dielectric constant that results from the extrapolation of the relatively high-frequency polariton measurements. We describe the indirect mean-field response as a Debye relaxational mode:[3]

$$\epsilon_{\mathrm{MF}}(\omega) = \frac{\alpha}{1 - i\omega\tau}, \qquad (3.4)$$

with α the indirect mean-field contribution to the static dielectric constant and τ a relaxation-time constant. The value of α is obtained by subtracting the static dielectric constant that results from the transitions in the unit cell from the dielectric constant that results from the self-consistent calculation of the value of $\langle r \rangle$ upon application of a static electric field. In the following we will refer to this response as central mode because the maximum response is attained at frequency zero. The contribution of the central mode to the dielectric constant is real at frequency zero, which can be expected since there will be no phase shift between a static electric field and the induced static polarization.

The total dielectric function that is given by the sum of Eqs. (3.3) and (3.4) is used to calculate the polariton response as defined by Barker and Loudon:[25]

$$R(k_p, \omega_p) = \mathrm{Im}\left\{\frac{1}{(c^2k_p^2/\omega_p^2) - \epsilon(\omega_p)}\right\}, \qquad (3.5)$$

with $\epsilon(\omega_p) = \epsilon_\infty + \epsilon_{\mathrm{SU}}(\omega_p) + \epsilon_{\mathrm{MF}}(\omega_p)$. The maxima of this response define the polariton dispersion. This definition leads to two different types of polariton-dispersion curves, depending on whether the maximum of this function is searched by varying ω_p at constant k_p or by varying k_p at constant ω_p. Especially for frequencies near the transition frequency of a damped resonance this leads to strongly different results. Which dispersion curve has to be compared with the experiment depends on how the experiment is performed. In our experiment the wave vector k_p is fixed and the frequency ω_p is obtained out of the bandwidth of the laser pulses so that in searching the maximum of the response, the value of ω_p should be varied at constant k_p.

The polariton response of Eq. (3.5) also defines the width of the response in k_p at a particular ω_p or the width of the response in ω_p at a particular k_p. The inverse of the width of the response in ω_p at a particular k_p defines the damping-time constant T_{2p} of the polariton. This damping-time constant should not be confused with the damping-time constants $T_{2,ij}$ of the vibrational transitions. When many resonances contribute to the dielectric function the polariton response becomes a complicated function of ω_p. As a result the damping of the polaritons can be strongly nonexponential.

IV. RESULTS AND DISCUSSION

We performed time-resolved measurements on phonon polaritons at five different temperatures: 300 K, 433 K, 533 K, 633 K, and 733 K. At each temperature measurements are carried out at many different wave vectors in order to determine the polariton dispersion and to measure the damping of the polaritons as a function of frequency. In Fig. 3, six examples of time-resolved measurements are shown. The dashed curves in Fig. 3 are the results of simulations in which the polaritons are described as damped Gaussian wave packets that propagate with the group velocity. For all measurements we observe an excellent agreement between experiment and simulation, indicating that all relevant phenomena are incorporated in the simulation.

In Fig. 3(a), a measurement is shown in which the probe is focused 250 μm next to the common focus of the two pump beams. As a result, we observe that the diffracted signal reaches its maximum after 5 ps, which is the time the polariton needs to propagate into optimum

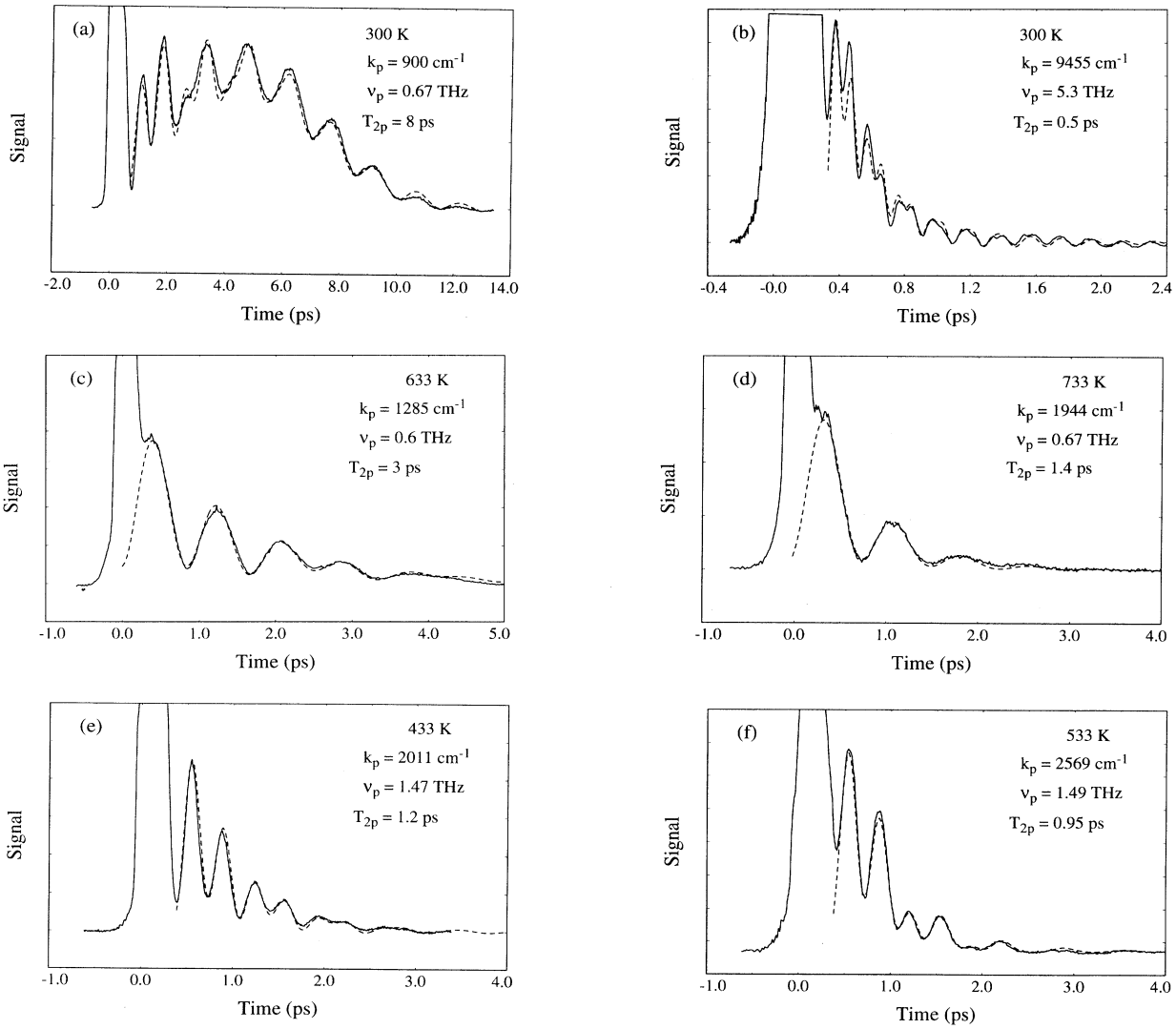

FIG. 3. Time-resolved measurements of the diffracted signal as a function of the delay between the probe and the two pump pulses. Six measurements are shown in which the wave vector, the temperature, and the position of the probe are varied. The damping-time constant T_{2p} of the polariton is determined via a simulation of the signal. This simulation is represented by the dashed curve.

overlap with the probe beam. The Gaussian shape of the signal results from the time dependence of the overlap of the envelope function of the polariton and the spatial profile of the probe. The signal is modulated at small delays with the double-polariton frequency due to the fact that the spatial profile of the probe overlaps with the tails of both generated counterpropagating polaritons. With increasing delay one of the polaritons propagates into better overlap with the probed area while the other propagates away from the probe spot so that at later delay times the double-polariton frequency is no longer observed. At later delay times we observe that the signal is modulated with the single-polariton frequency, indicating the presence of background scattered light that interferes with the diffracted electric field of the polaritons. At this low wave vector, the polariton frequency is far away from the phonon resonance at 6 THz. Therefore the polaritons have very little phonon character and are only weakly damped (T_{2p}= 8 ps), so that it is possible to observe one of the polaritons propagating through the probed area. We find that polaritons with frequencies below 2 THz can still be detected even after propagating several milimeters through the crystal.

In Fig. 3(b), a time-resolved measurement is shown obtained with a much larger wave vector. The polariton frequency of 5.3 THz approaches the value of the strong resonance at 6 THz so that the polaritons will have strong phonon character. In this experiment the probe was focused at the same spot as the two pump beams, so that the probe overlaps with both counterpropagating polaritons and mainly the double-polariton frequency is observed for small delays. As in Fig. 3(a), we observe a transition from the double-polariton frequency to the polariton frequency with increasing delay. This transition can not be due to propagation of the polaritons because at this frequency the decay of the signal as a result of propagation is totally negligible compared to the decay due to damping. However, as a result of the decay of the polariton, the interference with background scattered light becomes relatively more important at later delay times, since it follows from Eq. (2.7) that this signal is linearly proportional to the diffracted electric field whereas the signal that results from the diffraction from two interfering counterpropagating polaritons depends quadratically on the diffracted electric field. Figures 3(c,d) show that low-frequency polaritons that are practically not damped at 300 K become strongly damped at higher temperatures. In these experiments the probe is also focused at the same spot as the two pump beams. Figures 3(e,f) also show that the damping of the polariton increases with increasing temperature. These figures again show the transition from the double-polariton frequency at small delays to the polariton frequency at large delays as a result of the increasing relative importance of the interference with background scattered light.

We used the quantum-mechanical model of Sec. III to calculate self-consistently the values for the mean displacement of the ions and the static dielectric response at different temperatures. In this calculation we assume that only the dielectric response of the ferroelectric mode is temperature dependent. The contribution of the other phonons and electronic transitions is contained in ϵ_∞. We assume that this ϵ_∞ does not depend on temperature and that the temperature dependence of the dielectric response only results from the ferroelectric mode. This should be a good assumption, because Raman-scattering experiments show that of the phonon modes that contribute to the dielectric function only the ferroelectric mode strongly depends on temperature.[16] The results of the calculations are presented in Table I. The mean value of the normal vibrational coordinate is represented by the displacement of the Li^+ ion from the centrosymmetric position in the unit cell. The calculated results are in good agreement with the displacements derived from the measurement of the spontaneous polarization[26,27] and values of the static dielectric constant obtained with capacitance measurements.[28]

Equations (3.3) and (3.4) are used to calculate the dielectric function at the five temperatures of the experiment. The calculated real and imaginary parts of the dielectric function are presented in Fig. 4. In this calculation we used the transition-dipole moments, vibrational energies, and values for α that follow from the quantum-mechanical model. We used a value for $T_{2,ij}$ of 250 fs for all transitions at all temperatures. For the time constant τ of the central mode we also used a value of 250 fs. We calculate that with increasing temperature the resonance at 200 cm^{-1} (6 THz) becomes weaker and a new broad resonance rises near 100 cm^{-1} (3 THz). In addition, we calculate that at temperatures above 500 K the influence of the central mode becomes apparent at frequencies below 2 THz. For all temperatures, we find that transitions with frequencies of 6 THz correspond to transitions between low-energy vibrational levels that are localized in

TABLE I. Mean displacement and static dielectric response calculated with the quantum-mechanical model of Sec. III. The contribution of the direct single-unit-cell response [given by Eq. (3.3)] to the dielectric response is denoted with ϵ_{SU}, the contribution of the indirect mean-field response [given by Eq. (3.4)] with ϵ_{MF}. The experimental values for $\langle r \rangle$ and $\epsilon_{tot}(0)$ are obtained from Refs. 26 and 27, respectively.

Temperature	$\langle r_{Li^+} \rangle$	$\langle r_{Li^+} \rangle$ expt.	ϵ_∞	$\epsilon_{SU}(0)$	$\epsilon_{MF}(0)$	$\epsilon_{tot}(0)$	$\epsilon_{tot}(0)$ expt.
300 K	0.043 nm	0.043 nm	18	22	2	42	43
433 K	0.040 nm	0.040 nm	18	36	8	62	54
533 K	0.037 nm	0.037 nm	18	49	20	87	74
633 K	0.032 nm	0.032 nm	18	61	55	134	110
733 K	0.025 nm	0.025 nm	18	88	139	245	215
T_c	0.000 nm	0.000 nm	18	212	∞	∞	∞

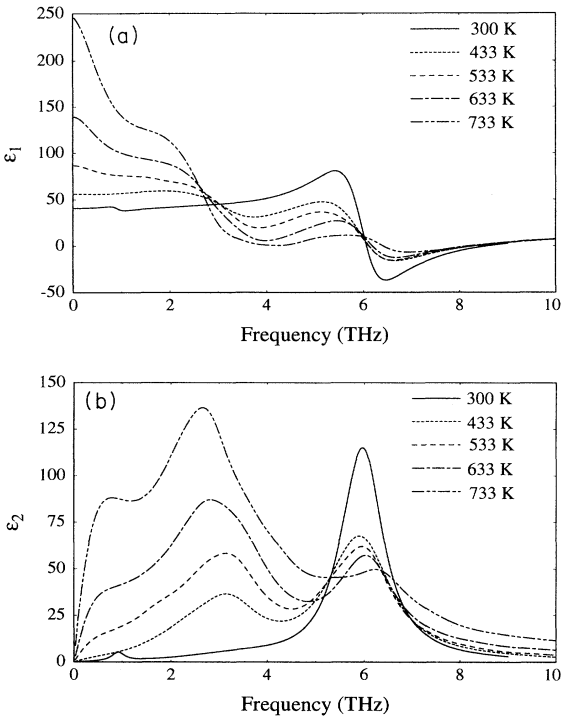

FIG. 4. Real (ϵ_1) and imaginary (ϵ_2) dielectric function as a function of temperature, calculated with the quantum-mechanical model of Sec. III for $LiTaO_3$. The relaxation-time constant of the central mode and the damping-time constant of the transitions in the potential are taken equal to 250 fs at all temperatures.

the lowest-energy well of the potential and that transitions with frequencies near 3 THz correspond to transitions between higher-energy delocalized levels. The rise of the latter resonance is caused by the increase of the population of these higher-energy delocalized levels with increasing temperature. The resonances near 3 THz and 6 THz are both very broad because they consist of many transitions.

We find that the resonance near 3 THz is already weakly present at 300 K. This resonance has been observed in previous experimental studies,[6,13,16,29] but has not been unambiguously assigned. It has been suggested that this resonance may be due to coupling of the A_1 phonon to the phonons of E symmetry at about the same frequency.[6,16] However, a Raman-scattering study showed that this resonance has pure A_1 character.[29] From the quantum-mechanical model it follows that this resonance is due to overtone absorption in the potential of the lowest-energy A_1 phonon. This resonance is thus a direct consequence of the anharmonic character of this phonon. This explanation also agrees with the fact that only four different fundamental A_1 modes exist in the ferroelectric phase in $LiTaO_3$ that have already been assigned to strong resonances of A_1 symmetry.[16]

The energy splitting of delocalized vibrational levels can become very small for vibrational energies near the maxima of the barriers that separate the three wells of the potential. Hence, in addition to the broad resonances at 3 and 6 THz, low-frequency tunneling transitions can arise that may have much smaller linewidths because they originate from a single transition. At 300 K the fifth and the sixth levels are delocalized over the middle and the lowest wells and have an energy splitting of only 32 cm^{-1} (1 THz). This energy difference depends on the height and width of the barrier between the two wells. Due to the small thermal population of these levels, only a weak resonance at 1 THz will arise in the spectrum. This resonance has recently been observed in a time-resolved study on phonon polaritons in $LiTaO_3$.[9] It can be interpreted as the oscillation of the Li^+ ion between the two wells. This oscillation is classically forbidden, since the energy of both delocalized vibrational states is smaller than the top of the barrier. Therefore this resonance is a tunneling resonance. At higher temperatures it is more difficult to observe tunneling resonances because with increasing temperature these resonances will become weaker due to the decrease of the population difference of the levels involved in the transition.

We use the calculated dielectric function to calculate the polariton response with Eq. (3.5). This calculated polariton response provides calculated values for the polariton dispersion and damping which can be compared with the experimental results. In Fig. 5 both the experimentally determined and the calculated polariton dispersions are presented for the five different temperatures of the experiment. The points represent the experimental data obtained from the Fourier transforms of the time-resolved measurements. The dashed curves in Fig. 5 represent the calculated maxima of the polariton response and the solid curve represents the simulated "experimental" dispersion. To be able to compare the calculated polariton dispersion with the experimental results, the characteristic features of the experiment have to be taken into account. There are two important effects that will influence the measured signal. The first effect is that the laser pulses have a limited bandwidth. This means that high-frequency polaritons are less efficiently excited than low-frequency polaritons. This effect is accounted for by multiplying the calculated polariton response with a Gaussian that represents the spectrum of the laser pulses. The second effect that has to be accounted for is that in an experiment in which the probe is focused close to the common focus of the two pump beams, the measured signal results from the diffraction from two interfering counterpropagating polaritons. To compare the calculated polariton response with the experiment, we used Eq. (2.11) to transform the calculated polariton response to the diffracted intensity that will result from the diffraction of a probe pulse from two counterpropagating polaritons. In the experiments in which the probe is diffracted from two counterpropagating polaritons, we did not observe a clearly resolved peak at low frequencies. This could mean that the polariton response has only one well-defined maximum or that this response consists of several broad and overlapping peaks. We interpreted both the maximum of the Fourier transform of the time-resolved measurement and the maximum of the Fourier transform of the signal that is calculated using Eq. (2.11) as the double-polariton frequency. If the

polariton response has only one maximum, the thus determined polariton frequency is indeed the maximum of the polariton response. If the polariton response contains several maxima, the polariton frequency does not correspond to one of these maxima but will still approximately equal the average polariton frequency.

The simulated and experimentally observed dispersions are in good agreement at all temperatures. At 300 K the dispersion is influenced by the weak tunneling resonance at 1 THz and the strong resonance at 6 THz. At higher temperatures we observe that for wave vectors below 5000 cm^{-1} the polariton frequency appears to saturate below 3 THz due to the rise of the broad resonance at this frequency. However, at 433 K and 533 K a jump in the polariton frequency is observed in both experiment and calculation and polaritons with frequencies above 3 THz are observed. The presence of the broad resonance at 3 THz leads to an avoided crossing in the polariton dispersion and to the formation of two polariton-dispersion branches, one below and one above 3 THz. The splitting between these branches increases with increasing strength of the resonance. In Fig. 6 the calculated polariton response at 533 K is presented as a function of wave vector and frequency. This figure shows that below 5000 cm^{-1} the lower dispersion branch has a much stronger response than the upper dispersion branch. Hence in this wave vector regime only the lower dispersion curve will be observed in the experiment. At wave vectors near 5000

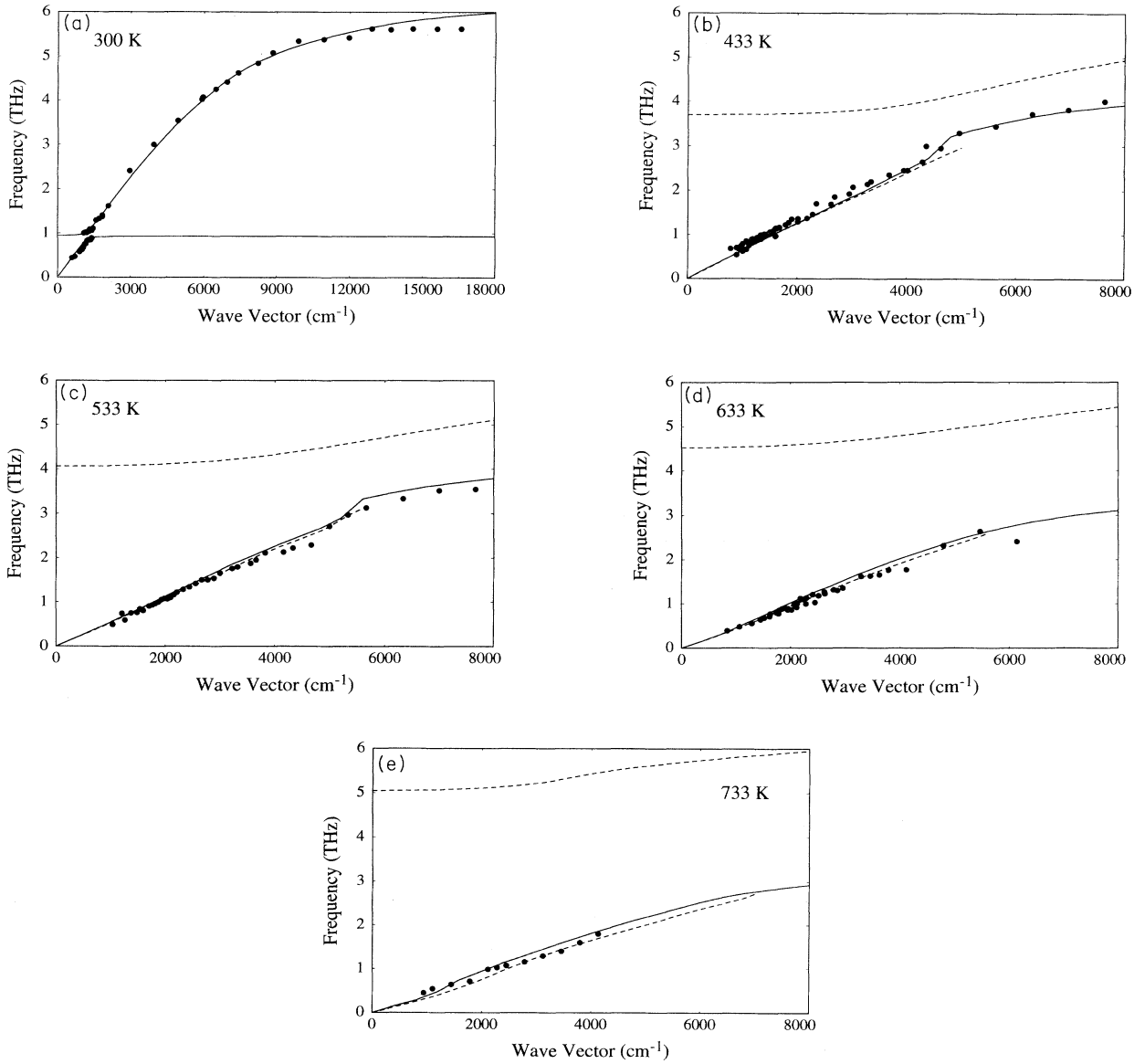

FIG. 5. Measured and calculated polariton dispersions at five different temperatures. The measurements are represented by points. The calculated maxima of the polariton response are represented by the dashed curves and the simulation of the experiment including the limited bandwidth of the laser pulses and the interference of the two counterpropagating polaritons is represented by the solid curve.

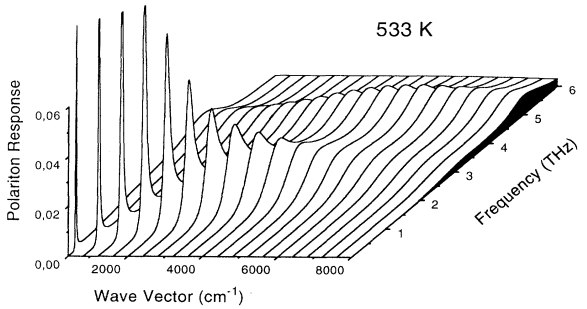

FIG. 6. Polariton response at 533 K as a function of wave vector and frequency calculated with the quantum-mechanical model of Sec. III.

cm^{-1}, the response of the lower dispersion branch decreases while the response of the upper polariton branch increases. This change in the polariton response leads to a shift of the maximum of the diffracted intensity of two counterpropagating polaritons from the double frequency of the lower dispersion branch to the sum frequency of the maxima of the lower and the upper dispersion branch. As a consequence, for wave vectors near 5000 cm^{-1}, the average polariton frequency rapidly shifts to higher values with increasing wave vector.

Figure 5 also shows that the polariton frequency at a particular wave vector decreases with increasing temperature. This indicates that the static dielectric constant derived from the polariton dispersion increases with temperature. This observation can easily be explained with the quantum-mechanical model. At higher temperatures higher vibrational levels in the potential become occupied that have low transition frequencies and have larger transition dipole moments due to their delocalization. Both effects lead to a large contribution of these transitions to the static dielectric constant. Hence the increase in the static dielectric constant as observed in the dispersion of polaritons with frequencies above 0.5 THz can be fully explained from the change in the direct single-unit-cell response with increasing temperature. We observe both in experiment and in calculation that the indirect mean-field dielectric response formed by the central mode has very little effect on the polariton dispersion, at least for temperatures up to 733 K.

The calculated polariton response is also used to evaluate the frequency-dependent damping time of the polaritons. In Fig. 7 the experimental and calculated polariton damping-time constants are presented as a function of frequency, assuming this damping to be exponential. The points represent the measured results and are obtained from a numerical simulation of the time-resolved measurements including the effects of damping, propagation, and interference. The dashed curve represents a quantum-mechanical calculation of T_{2p} without central mode and the solid curve represents a quantum-mechanical calculation of T_{2p} with central mode. At 300 K we observe that for frequencies below 2 THz the polaritons are practically undamped. For frequencies above 2 THz the damping becomes significant and slowly increases on approaching the strong resonance frequency at 6 THz. This frequency dependence of the damping indicates the presence of a weak and broad resonance near 3 THz at 300 K. If this resonance would be absent, the polaritons would have been practically undamped up to frequencies of about 4 THz.

At higher temperatures the damping increases as a result of the rise of the broad resonance near 3 THz and the central mode. We only present measurements of the damping time for frequencies below 2.5 THz. At higher frequencies the damping becomes highly nonexponential as a result of the complicated structure of the polariton response. The difference between the solid curves and the dashed curves in Fig. 7 shows the strong effect of the central mode on the damping of polaritons with frequencies below 3 THz. We find that for temperatures above 500 K the central mode is essential to obtain quantitative agreement between experiment and calculation. The value of the relaxation-time constant of the central mode of 250 fs does not depend on temperature and agrees very well with values measured in a cw Raman-scattering study on the central mode of $LiTaO_3$.[3] It is also similar to the relaxation-time constant of the central mode measured for the related ferroelectric $KNbO_3$.[5,30] In these studies on $KNbO_3$ it is observed that the relaxation-time constant is almost temperature independent for temperatures far below T_c and decreases with increasing temperature for temperatures close to T_c. The maximum temperature of 733 K of our experiment is still rather far away from the Curie temperature of 890 K. This explains why our measurements can be fitted with a relaxation-time constant for the central mode that does not depend on temperature in the temperature interval studied in our experiment.

Up to now it has been very hard to determine experimentally whether the ferroelectric phase transition in $LiTaO_3$ takes place with or without the frequency of the lowest-energy A_1 mode gradually shifting to zero (mode softening).[3,16–18] In the quantum-mechanical model the divergence of the static dielectric constant follows from the divergence of the indirect mean-field response at the Curie temperature. Instead of a gradual shift of the transition frequency to zero, this model predicts a change in the resonance frequency from 6 THz to 3 THz and a rise of a strong central mode for temperatures near the Curie temperature. In Raman-scattering or infrared-reflectivity experiments this change in the resonance frequency and the rise of a central mode may give the impression that the ferroelectric phase transition takes place with mode softening.[16,17] We find that the time-resolved measurement of the polariton dispersion and damping provides detailed information on the temperature dependence of the ferroelectric mode and we conclude from the good agreement between model and experiment that the ferroelectric phase transition in $LiTaO_3$ takes place without mode softening.

V. CONCLUSIONS

The low-frequency dielectric response of $LiTaO_3$ has been investigated in detail with time-resolved measure-

ments of the phonon-polariton dynamics. Counterpropagating phonon polaritons with well-defined wave vector and phase are effectively excited via nonlinear interaction of two ultrashort laser pulses with equal central frequency. The polaritons are probed by diffracting a probe beam from the index grating that is formed by the polaritons via the linear electro-optic effect. The experimentally measured signals are influenced by the interference of the diffracted electric field with background scattered light, the interference of the two counterpropagating polaritons, and the interference due to the excitation of two or more polariton-dispersion branches. The damping-time constant of the polaritons is determined by a simulation of the experiment in which the polaritons are described as damped propagating Gaussian wave packets.

The low-frequency dielectric response of $LiTaO_3$ is theoretically described with a quantum-mechanical model in which the vibrational levels of the lowest-energy A_1 phonon are calculated. This model uses a potential that is adjusted to the positions of the Li^+ ion in the unit cell above T_c and to the absorption spectrum at 300 K. The model predicts a decrease of the strength of the resonance at 6 THz, a rise of a central mode and a rise of a broad resonance near 3 THz with increasing temperature. The latter resonance is due to overtone absorption in the one-dimensional anharmonic triple-well potential that describes the lowest-energy A_1 mode in a single unit cell. The model predicts that the static dielectric response diverges at the Curie temperature without the resonance frequency of the lowest-energy A_1 mode of $LiTaO_3$ gradually shifting to zero. We find that with

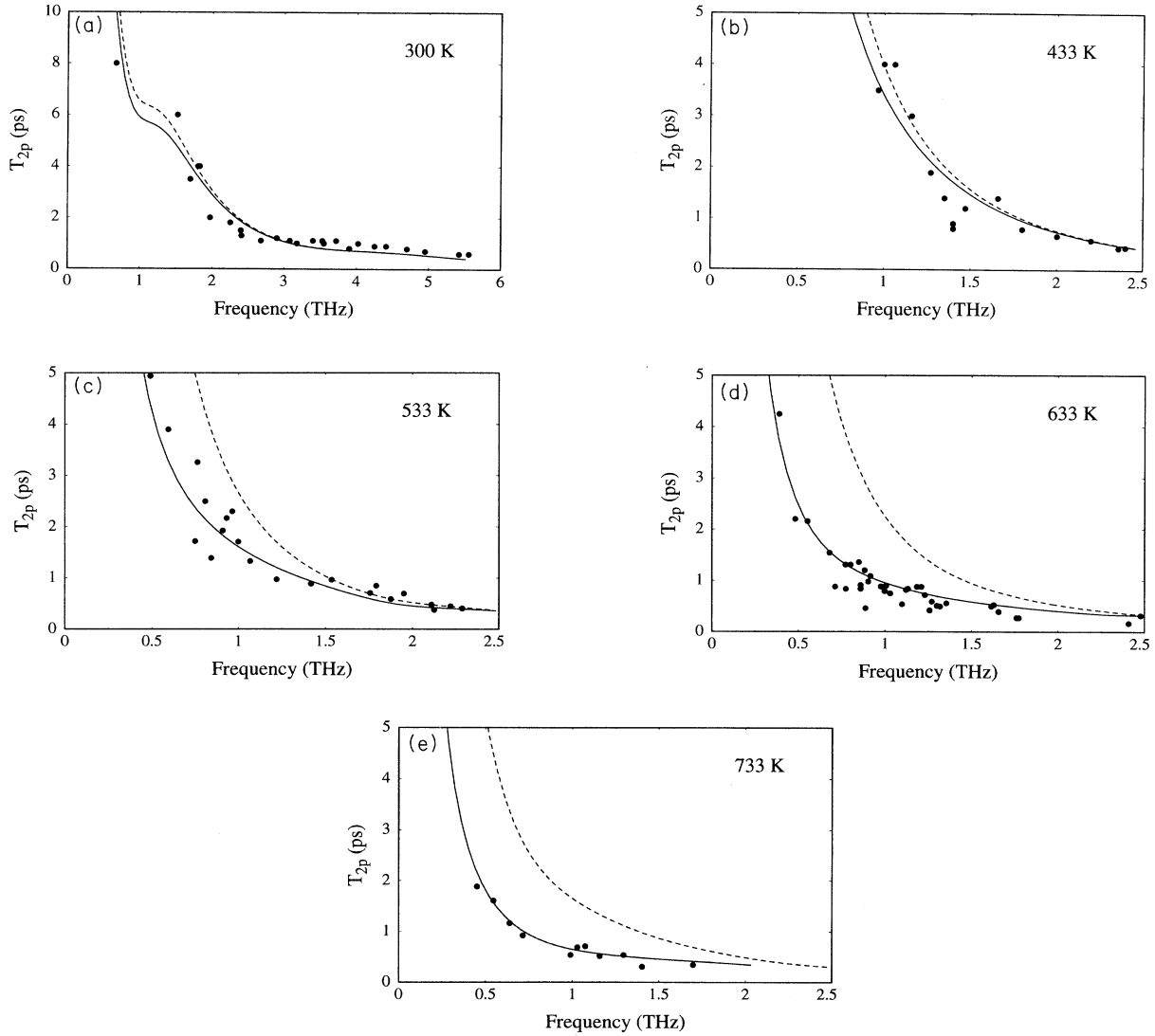

FIG. 7. Measured and calculated polariton damping-time constants at five different temperatures. The measurements are represented by points. The dashed curve represents the calculation of the damping-time constant from the width of the peak in the calculated polariton response without the central mode. The solid curve represents the calculation of the damping-time constant with the central mode.

frequency- and temperature-independent time constants of 250 fs for the central mode and the damping of each transition in the potential, the model provides a quantitative description of the polariton dispersion and damping in $LiTaO_3$ at all temperatures. Thereby we obtain strong evidence that the ferroelectric phase transition in $LiTaO_3$ takes place without mode softening. We also deduce from the comparison between the measured and the calculated polariton damping that the central mode strongly affects the damping of polaritons with frequencies below 3 THz.

ACKNOWLEDGMENT

We thank K. Elbern for experimental assistance.

[1] C. Kittel, *Introduction to Solid-State Physics*, 6th ed. (Wiley, New York, 1986).
[2] A. F. Penna, S. P. S. Porto, and E. Wiener-Avnear, Solid State Commun. **23**, 377 (1976).
[3] A. F. Penna, A. Chaves, and S. P. S. Porto, Solid State Commun. **19**, 491 (1976).
[4] S. Kojima and T. Nakamura, Ferroelectrics **37**, 677 (1981).
[5] T. P. Dougherty, G. P. Wiederrecht, and K. A. Nelson, Ferroelectrics **120**, 79 (1991).
[6] T. P. Dougherty, G. P. Wiederrecht, and K. A. Nelson, J. Opt. Soc. Am. B **9**, 2179 (1992).
[7] T. P. Dougherty, G. P. Wiederrecht, K. A. Nelson, M. H. Garret, H. P. Jensen, and C. Ward, Science **258**, 770 (1992).
[8] J. Etchepare, G. Grillon, A. Antonetti, J. C. Loulergue, M. D. Fontana, and G. E. Kugel, Phys. Rev. B **41**, 12 362 (1990).
[9] H. J. Bakker, S. Hunsche, and H. Kurz, Phys. Rev. Lett. **69**, 2823 (1992).
[10] P. C. M. Planken, L. D. Noordam, J. T. M. Kennis, and A. Lagendijk, Phys. Rev. B **45**, 7106 (1991).
[11] G. M. Gale, F. Valleé, and C. Flytzanis, Phys. Rev. Lett. **57**, 1867 (1986).
[12] F. Valleé and C. Flytzanis, Phys. Rev. B **46**, 13799 (1992).
[13] K. P. Cheung and D. H. Auston, Phys. Rev. Lett. **55**, 2152 (1985); D. H. Auston and M. C. Nuss, IEEE J. Quantum Electron. **QE-24**, 184 (1988).
[14] D. Fröhlich, A. Kulik, B. Uebbing, A. Mysyrowicz, V. Langer, H. Stolz, and W. von der Osten, Phys. Rev. Lett. **67**, 2343 (1991).
[15] P. C. M. Planken, Ph.D. thesis, University of Amsterdam, 1991.
[16] W. D. Johnston, Jr. and I. P. Kaminow, Phys. Rev. **168**, 1045 (1968).
[17] J. L. Servoin and F. Gervais, Solid State Commun. **31**, 387 (1979).
[18] M. R. Chowdhurry, G. E. Peckman, and D. H. Saunderson, J. Phys. C **11**, 1671 (1978).
[19] H. J. Bakker, S. Hunsche, and H. Kurz, Phys. Rev. B **48**, 9331 (1993).
[20] W. H. Knox, IEEE J. Quantum Electron. **QE-24**, 388 (1988).
[21] J. W. Flocken, R. A. Guenther, J. R. Hardy, and L. L. Boyer, Phys. Rev. B **40**, 11496 (1989).
[22] S. C. Abrahams, E. Buehler, W. C. Hamilton, and S. J. Laplaca, J. Phys. Chem. Solids **34**, 521 (1973).
[23] M. E. Lines, Phys. Rev. **177**, 797 (1969); **177**, 812 (1969); **177**, 819 (1969).
[24] G. Dahlquist, A. Björck, and N. Anderson, *Numerical Methods* (Prentice-Hall, New York, 1974).
[25] A. S. Barker, Jr. and R. Loudon, Rev. Mod. Phys. **44**, 18 (1972).
[26] S. C. Abrahams and J. L. Bernstein, J. Phys. Chem. Solids **28**, 1685 (1967); S. C. Abrahams, W. C. Hamilton, and A. Sequeira, *ibid.* **28**, 1693 (1967).
[27] H. Iwasaki, N. Uchida, and Y. Yamada, Jpn. J. Appl. Phys. **6**, 1336 (1967).
[28] T. Yamada, N. Niizeki, and H. Toyoda, Jpn. J. Appl. Phys. **7**, 292 (1968).
[29] A. F. Penna, A. Chaves, P. da R. Andrade, and S. P. S. Porto, Phys. Rev. B **13**, 4907 (1976).
[30] J. P. Sokoloff, L. L. Chase, and D. Rytz, Phys. Rev. B **38**, 597 (1988).